Mon. Not. R. Astron. Soc. **371,** 633–642 (2006) doi:10.1111/j.1365-2966.2006.10461.x

Radial kinematics of isolated elliptical galaxies

G. K. T. Hau[1]★ and Duncan A. Forbes[2]

[1]*Department of Physics, University of Durham, South Road, Durham DH1 3LE*
[2]*Centre for Astrophysics and Supercomputing, Swinburne University of Technology, Hawthorn, VIC 3122, Australia*

Accepted 2006 April 19. Received 2006 March 16; in original form 2005 December 24

ABSTRACT

Ellipticals in very low-density environments are extremely rare but hold important clues about galaxy formation and evolution. In this paper, we continue our study of isolated elliptical galaxies, presenting results on the radial stellar kinematics for 13 isolated early-type galaxies. We derive radial rotation velocity, velocity dispersion and hermite terms to $\sim$1 effective radius. We observe a dichotomy in kinematic properties similar to that in the elliptical population as a whole, where low-luminosity ellipticals tend to be rotationally supported. For all galaxies the V/σ ratio increases with radius. We find kinematically distinct cores (KDCs), or velocity substructure, in $\sim$40 per cent of the galaxies for which we have major axis spectra. Such a fraction is similar to that observed for ellipticals in higher-density environments. Most galaxies in the sample reveal kinematic evidence for a nuclear disc. The non-relaxed kinematics in several galaxies suggests that they have undergone a merger or accretion event. Isolated ellipticals generally follow the Fundamental Plane defined by cluster ellipticals – exceptions being those galaxies with evidence for young stellar populations. Overall, we find isolated ellipticals have similar kinematic properties to their counterparts in higher-density environments.

Key words: galaxies: elliptical and lenticular, cD – galaxies: fundamental parameters – galaxies: general – galaxies: kinematics and dynamics.

1 INTRODUCTION

Galaxies are found in three broad environments, defined in terms of their spatial density. These range from clusters with hundreds of galaxies within a few Mpc, to groups to relatively isolated galaxies (the 'field'). The local environment is thought to play a key role in galaxy formation and subsequent evolution.

It is relatively easy to study large numbers of cluster galaxies because a single CCD image or spectral mask may contain hundreds of galaxies. For low-density environments, the same CCD may contain only one or two bright galaxies. Consequently, our knowledge of the nearby Universe is often directly proportional to the environmental density. Very isolated galaxies (sometimes called the 'extreme field') are consequently the least studied and understood.

Although poorly studied, this extreme in the density range of galaxy environments offers crucial 'leverage' to tackle several outstanding issues in galaxy evolution. For example, the current hierarchical models for galaxy formation predict that ellipticals in low-density environments have younger mean stellar populations and lower [Mg/Fe] ratios than their cluster counterparts (e.g. Kauffmann & Charlot 1998; Kuntschner et al. 2002; Nagashima et al. 2005; de Lucia et al. 2006). Under this framework, isolated ellipticals are thought to have formed in relatively recent mergers of spiral galaxy pairs. If so, we might expect a high incidence of kinematical misalignments (Weil & Hernquist 1996), such as kinematically distinct cores (KDCs). Alternatively, large isolated ellipticals may be the result of a merged small group of galaxies (D'Onghia et al. 2005; Jones, Ponman & Forbes 2000). Here, we might expect an increasing importance of rotation with galactocentric radius and rotation about the minor axis (Weil & Hernquist 1996).

Kuntschner et al. (2002) studied a sample of nine early-type galaxies, selected from Southern Sky Survey plates, in low-density environments (i.e. $\leqslant$2 neighbours within 1.3 Mpc). Their CCD imaging revealed most of the galaxies to be morphologically disturbed; six of the nine are listed in the Arp-Madore catalogue of peculiar galaxies. They obtained long-slit spectra of the galaxies at the MSSSO 2.3-m telescope. They concluded that their sample galaxies were 2–3 Gyr younger and 0.2 dex more metal-rich than E/S0 galaxies in the Fornax cluster. The [Mg/Fe] ratio was similar to the Fornax galaxies. They did not explore the internal kinematics of their sample. The imaging study of nine isolated early-type galaxies by Marcum, Aars & Fanelli (2004) found a range of galaxy colours and morphologies – with some galaxies suggestive of being a recent merger remnant, while others appeared to be undisturbed and pristine.

In Reda et al. (2004), we defined a new sample of isolated galaxies. Briefly, early-type galaxies outside of groups and clusters, with $B_T \leqslant 14$, were selected from the LEDA data base. These were further restricted to have no neighbours within 700 km s^{-1} in velocity, 0.67 Mpc on the sky and two B-band magnitudes. Finally,

★E-mail: george.hau@durham.ac.uk

a visual check using the Digital Sky Survey (DSS) was carried out. This resulted in a sample of 36 very isolated E/S0 galaxies. Wide-field imaging of this sample is reported in Reda et al. (2004). Like Kuntschner et al. (2002) and Marcum et al. (2004), Reda et al. (2004) found several isolated galaxies to have signs of recent morphological disturbance.

In a second paper, Reda, Forbes & Hau (2005) examined the location of isolated galaxies on the Fundamental Plane (FP) using their photometric properties and central velocity dispersions. Most of the samples were found to lie on the FP as defined by cluster ellipticals. However, a small number of morphologically disturbed isolated galaxies deviated strongly from the FP in a direction consistent with their younger stellar populations (e.g. Forbes, Ponman & Brown 1998).

Here, we present new long-slit spectra of 13 isolated galaxies from the sample of Reda et al. (2004) and investigate their radial kinematic properties. A future paper will explore radial stellar population trends for these galaxies.

2 OBSERVATIONS AND DATA REDUCTION

2.1 Observations

A subsample of 13 isolated ellipticals from Reda et al. (2004) were observed over two observing runs (i.e. 2002 January 16–18 and 2004 December 11 and 12) using EFOSC2 at the ESO 3.6 m on the La Silla Observatory. The observational set-up for the runs are given in Table 1. The exposure times were 2×1200 s for the 2002 run, and 3×1200 s for the 2004 run.

For the elliptical galaxies we generally placed the slit along the major axis, but for the S0 galaxy ESO 153−G003 we chose to avoid the disc and hence aligned the slit along the minor axis. For NGC 1162 where no preferred axis was obvious, we choose the parallactic angle. The observed position angle (PA) of the slit is given, along with properties of the galaxy sample in Table 2.

Lick and spectrophotometric standards stars were taken at the parallactic angle. The Lick stars are also used for velocity standards. The spectrophotometric standards were taken with a 5-arcsec wide slit.

2.2 Data reduction

The data have been reduced using tasks within IRAF. After bias-subtraction, the pixel-to-pixel response variation was corrected using dome flats. The wavelength calibration is good to within 0.5 Å or 29 km s^{-1} rms. The data were corrected for instrumental response and spatial distortion and rebinned to logarithmic wavelength for the kinematic analysis. Special attention was taken with the slit-transfer function. This was estimated using dome flats which give a more uniform background than the twilight flats which are more prone to scattered light due to the open nature of the telescope. The sky background was determined from regions of the 2D spectrum far from the galaxy centre and subtracted from the final data.

Table 1. EFOSC2 observing characteristics.

	Run 1 (2002)	Run 2 (2004)
Chip	Loral/Lesser	Loral/Lesser
Chip size (pixels)	2048 × 2048	2048 × 2048
Binning	2 × 2	2 × 2
Pixel scale (binned pixel)	0.314 arcsec	0.314 arcsec
Read noise (e$^-$ binned pixel^{-1})	9.2	10.3
Gain (e$^-$ ADU^{-1})	1.33	1.17
Grism#	8	8
Lines mm^{-1}	600	600
Grism resolution FWHM	9.3 Å	7.8 Å
Wavelength coverage	4320–6360 Å	4320–6360 Å
Slit width	1.5 arcsec	1.2 arcsec

3 KINEMATIC ANALYSIS

Kinematic analysis was performed on logarithmically binned data, using van der Marel's code (van der Marel 1994). This code first finds the best-fitting mean velocity and dispersion for a Gaussian LOSVD, and then calculates the higher-order moments such as the third- and fourth-order Hermite terms (h_3 and h_4). These terms measure asymmetric and symmetric deviations from a Gaussian profile, respectively (van der Marel & Franx 1993). Note that although we present the h_3 and h_4 terms, the velocity and velocity dispersions are recovered independent of them.

Possible emission lines of [H II], [O III] and [N I] (even if no emission line is visible), the Hβ and Hγ lines and any pixels where the sky is strong are masked from the fitting. To arrive at the final values, the pixels which are 4–5σ from the mean in the residual spectrum are rejected, and this process is reiterated until a stable solution is obtained. This helps to reject hidden emission lines and bad columns or pixels.

3.1 Template matching

Template matching is important for the recovered kinematics as the line profiles can be sensitive to the choice of template. A number of stars have been observed with the same instrumental set-up as the galaxy observations. These are: HD15772 (K2III), HD36003 (K5V), HR2429 (K1III), HR2574 (K4III), HR3428 (G9III), HR4287 (K1III) and HR4657 (F5V). The latter three are also Lick standards. Template mismatch is minimized by comparing the χ^2 values from the LOSVD fitting using different stars. For each galaxy, a spectrum with signal-to-noise ratio (S/N) of 100–140 which encompasses a region of 1.6–12 arcsec, depending on the galaxy, was extracted and compared with each template in turn. The best template with the lowest average χ^2 is chosen. HR 2574 gave the best fits for all galaxies, and is used for the final data analysis. Further optimization was done by an iterative process to reject pixels which deviate too much from the fitted model.

3.2 Stellar dispersion measurements

We measure velocity dispersions according to the prescription of Jørgensen, Franx & Kjærgaard (1995). They used an aperture correction based on empirical kinematic models. Below we quote the equation which gives a distance-independent central velocity dispersion by correcting for the fact that an aperture of fixed angular size samples a larger portion of a radial velocity profile within a more distant galaxy.

$$\log\left(\frac{\sigma_{\rm ap}}{\sigma_{\rm norm}}\right) = -0.04\log\left(\frac{r_{\rm ap}}{r_{\rm norm}}\right). \quad (1)$$

Here, $\sigma_{\rm ap}$ is the velocity dispersion measured in a circular aperture of radius $r_{\rm ap}$, the 'normalized' velocity dispersion $\sigma_{\rm norm}$ is measured in the normalization radius $r_{\rm norm}$, i.e. $2r_{\rm norm} = 3.4$ arcsec for a galaxy at the distance of Coma.

Table 2. The observed sample. The Hubble T-type, Virgo infall and corrected velocity $V_{\rm Virgo}$ are from Hyperleda. The B-band absolute magnitude M_B is calculated from the apparent magnitude and foreground extinction A_B from Hyperleda, and velocity assuming $H_0 = 75\,{\rm km\,s^{-1}\,Mpc^{-1}}$. The B-band surface brightness is from Reda et al. (2005). The PAs of the slits are defined such that distances along the slit increase in the direction of the PA on the sky. The galaxy PA is estimated from DSS images. The ellipticity is taken either from Reda et al. (2004, 2005) or from Hyperleda. Runs 1 and 2 correspond to 2002 and 2004, respectively.

Galaxy	Right ascension (J2000)	Declination (J2000)	T	$V_{\rm Virgo}$ (km s^{-1})	M_B (mag)	A_B (mag)	$R_{\rm e}$ (arcsec)	$\langle\mu_{\rm e}\rangle$ (mag arcsec^{-2})	Slit PA (°)	Galactic PA (°)	Ellipticity	Run
ESO 153−G003	01 58 18.2	−54 12 57	−3.9	6242	−20.12	0.12	10.2	20.6	291	21	0.5	2
ESO 218−G002	12 21 09.3	−52 35 08	−3.9	4072	−20.62	0.75	20.1	21.5	187	3	0.15	1
ESO 318−G021	10 53 05.2	−40 19 46	−4	4641	−20.71	0.35	21.7	21.7	301	121	0.3	1
NGC 682	01 49 4.6	−14 58 29	−2.9	5456	−19.95	0.07	–	–	321	96	0.3	2
NGC 1045	02 40 29.1	−11 16 39	−3.0	4496	−20.63	0.19	16.7	20.8	238	58	0.3	2
NGC 1162	02 58 56.0	−12 23 55	−5.0	3789	−20.22	0.20	–	–	280	51	0.1	2
NGC 2110	05 52 11.4	−07 27 24	−3	2065	−19.82	1.62	24.3	20.7	345	345	0.2	1
NGC 2271	06 42 52.2	−23 28 32	−3.2	2402	−19.86	0.53	19.0	20.9	269	84	0.3	1
NGC 2865	09 23 30.7	−23 09 48	−4.1	2472	−20.35	0.36	27.7	20.8	333	153	0.2	1
NGC 4240	12 17 24.3	−09 57 07	−4	1916	−18.87	0.23	–	–	276	103	0.1	1
MCG-01-27-013	10 32 12.3	−9 14 22	−3	9044	−20.90	0.19	13.8	22.0	191	11	0.45	1
MCG-02-13-009	04 48 12.7	−13 40 03	−4	5494	−20.74	0.42	–	–	329	149	0.1	1
MCG-03-26-030	10 11 19.0	−17 12 17	−3	8948	−21.50	0.22	15.6	21.4	284	104	0.25	1

Using a library of kinematic data, they modelled the correction for $\sigma_{\rm ap}$ measured in a rectangular aperture of size $x \times y$ to that measured in a circular aperture of radius $r_{\rm ap}$.

$$2r_{\rm ap} \approx 1.025 \times 2\left(\frac{xy}{\pi}\right)^{1/2}. \quad (2)$$

We chose to measure the sigma inside a rectangular aperture of size $1.5 \times 5\,{\rm arcsec}^2$ for the 2002 data, and $1.2 \times 5\,{\rm arcsec}^2$ for the 2004 data, inside which the spectra are summed. The length of 5 arcsec along the slit is chosen such that it is at least three times the measured seeing. The corresponding $r_{\rm ap}$ is 1.584 arcsec. For the 1.2 × 5-arcsec^2 aperture, the $r_{\rm ap}$ is 1.417 arcsec.

Using equations (1) and (3) we can then relate the dispersion measured in a square aperture to the normalized dispersion. For each spectrum, we apply the kinematic analysis as described above. We choose to fit over the spectrum from $\lambda = 4420$ to 6280 Å. The regions corresponding to within 3σ of an emission line or the Hβ and Hγ lines are excluded (even if there is no emission). At the end of each fit, the s.d. in the noise-weighted residuals is calculated. If a pixel has a value more than 3 s.d. from the fitted model, it is excluded from the next fit. The process is repeated until a stable solution is obtained. The resulting $\sigma_{\rm norm}$ values and S/N are listed in Table 3.

4 KINEMATICS OF INDIVIDUAL GALAXIES

Before presenting our kinematic profiles we briefly discuss the interpretation of the h_3 and h_4 terms (see van der Marel & Franx 1993 for further details). As mentioned earlier, the hermite terms quantify deviations from a simple Gaussian velocity distribution. If the galaxy has a large-scale kinematic coherence then we expect symmetry (or antisymmetry) about the galaxy centre. Simple equilibrium models may then be applicable for the galaxy's kinematics. For the h_4 term we expect the profile to be similar on both sides of galaxy, whereas for h_3 we expect a reflection about an angle of 45°, i.e. positive one side and negative the other side of the galaxy centre. Embedded discs can be detected in the kinematic profiles; expected properties include a smooth antiasymmetric velocity profile with flat or declining velocity dispersion with radius, antisymmetric h_3 profile and weak h_4 term. Small systematic offsets are often seen in the h_4 term. This is due to the sensitivity of this term to continuum subtraction. The profiles in the central galaxy regions can be smeared out due to seeing effects, so any dips should be interpreted with caution.

In Figs 1–4 we show the velocity, velocity dispersion, h_3 and h_4 radial profiles along the slit direction. Below, we briefly discuss these kinematic radial profiles for each galaxy and summarize galaxy information from our previous imaging studies (Reda et al. 2004, 2005) and from NASA/IPAC Extragalactic Database (NED).

4.1 ESO 153−G003

Classified as an S0 galaxy in NED, ESO 153−G003 reveals a thin dust lane along the major axis and may actually be an edge-on Sa galaxy.

Table 3. Central velocity dispersion measurements. Values are derived from spectra extracted over the central 5 arcsec along the slit to match a standard aperture of 3.4 arcsec for a galaxy at the distance of Coma. $\sigma_{\rm norm}$ is the dispersion extracted from a fixed aperture of 5.0×1.5 or $5.0 \times 1.2\,{\rm arcsec}^2$ and normalized using the aperture prescription of Jorgensen et al. (1995). S/N is the signal-to-noise ratio of the extracted spectrum.

Galaxy	$\sigma_{\rm norm}$ (km s^{-1})	S/N
ESO 153−G003	223.5 ± 2.9	170
ESO 218−G002	284.1 ± 3.3	136
ESO 318−G021	244.4 ± 3.0	148
NGC 682	203.9 ± 1.8	235
NGC 1045	269.2 ± 1.8	260
NGC 1162	209.1 ± 1.8	235
NGC 2110	253.8 ± 4.0	145
NGC 2271	248.6 ± 3.0	142
NGC 2865	176.8 ± 1.8	288
NGC 4240	120.4 ± 2.3	194
MCG-01-27-013	246.6 ± 3.5	123
MCG-02-13-009	233.9 ± 3.5	125
MCG-03-26-030	318.1 ± 3.6	152

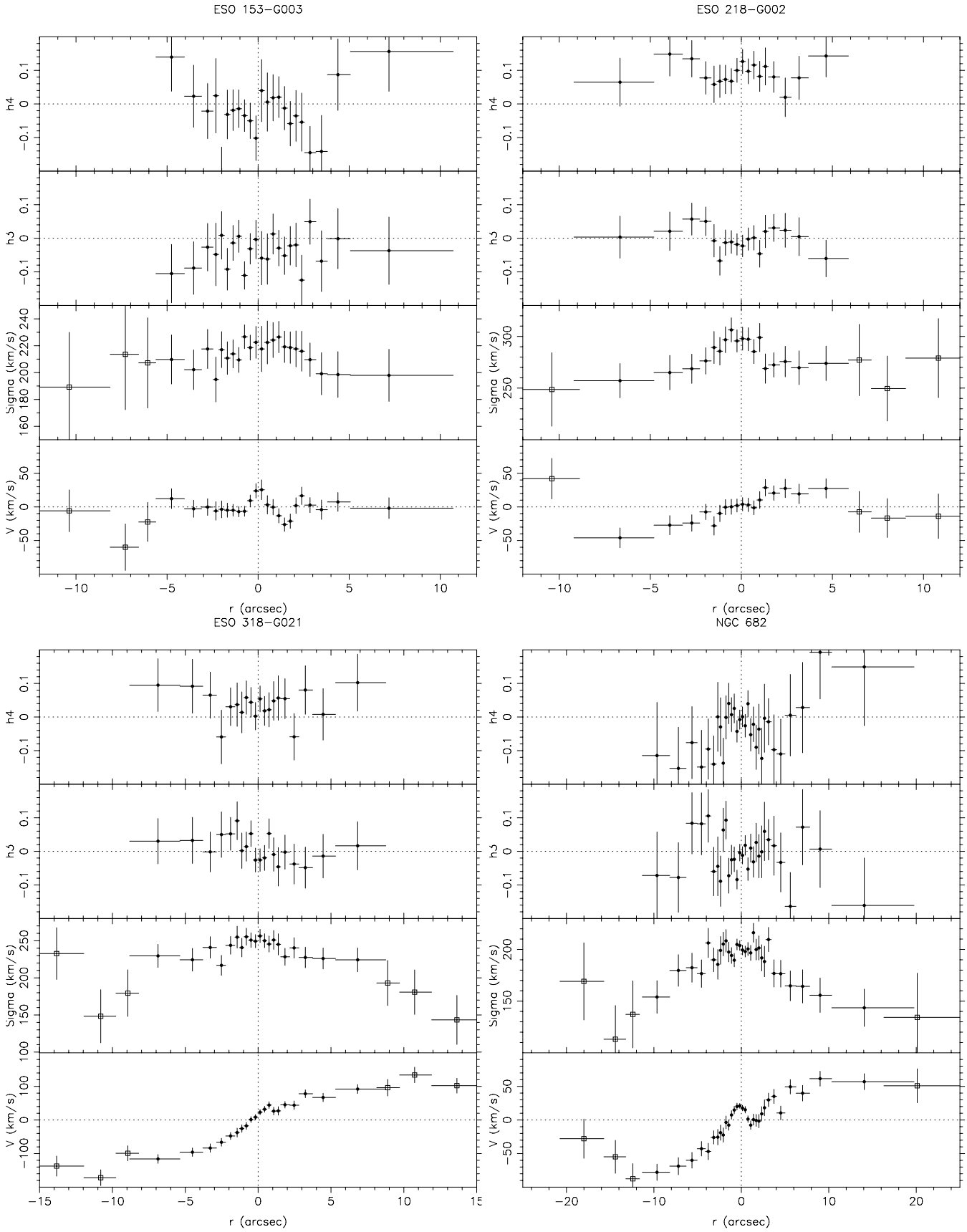

Figure 1. Radial kinematic profiles of isolated galaxies. From bottom to top are shown rotation velocity, velocity dispersion, third and fourth hermite terms. The open symbols indicate lower-S/N data for which we do not calculate hermite terms.

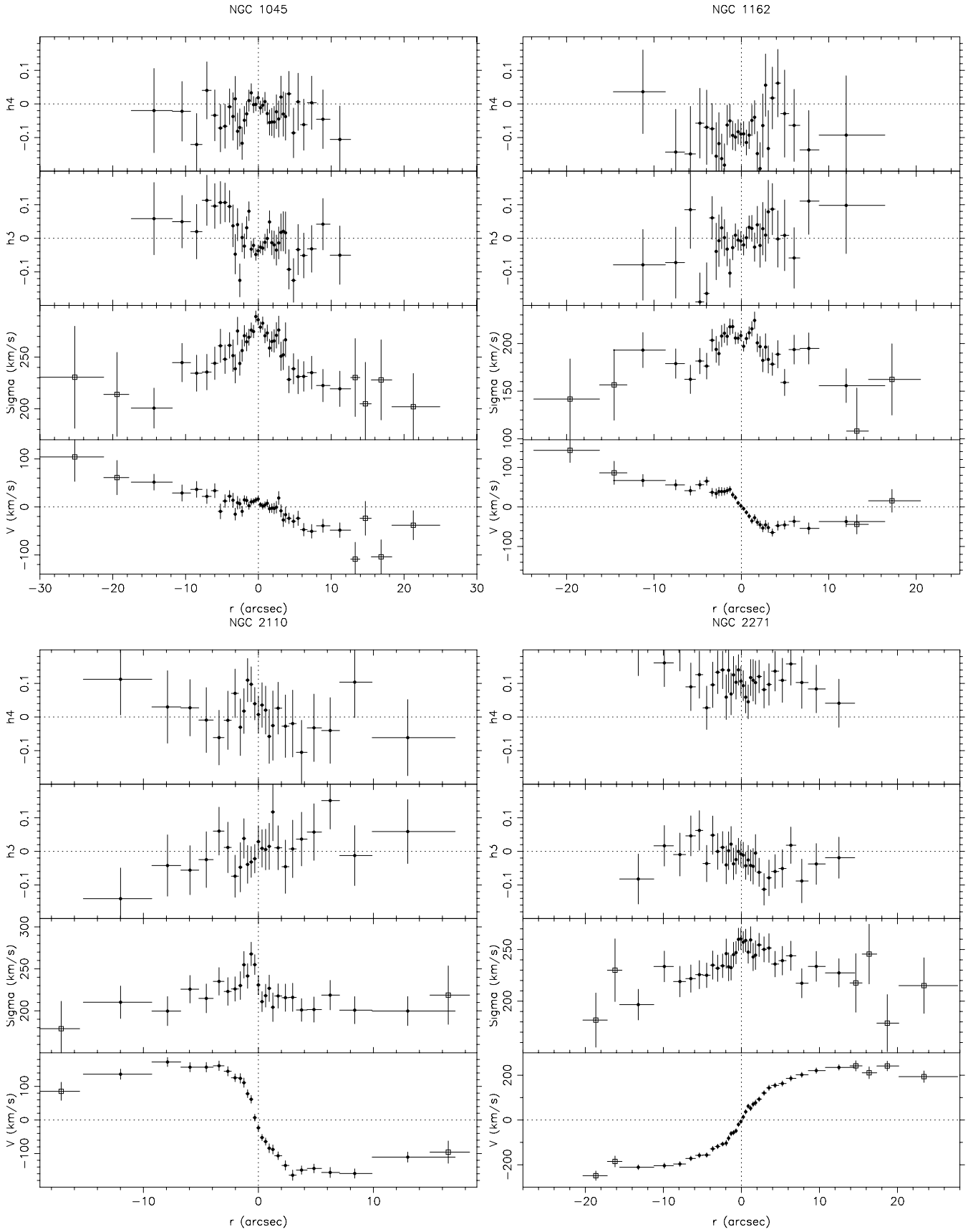

Figure 2. Radial kinematic profiles of isolated galaxies. From bottom to top are shown rotation velocity, velocity dispersion, third and fourth hermite terms. The open symbols indicate lower-S/N data for which we do not calculate hermite terms.

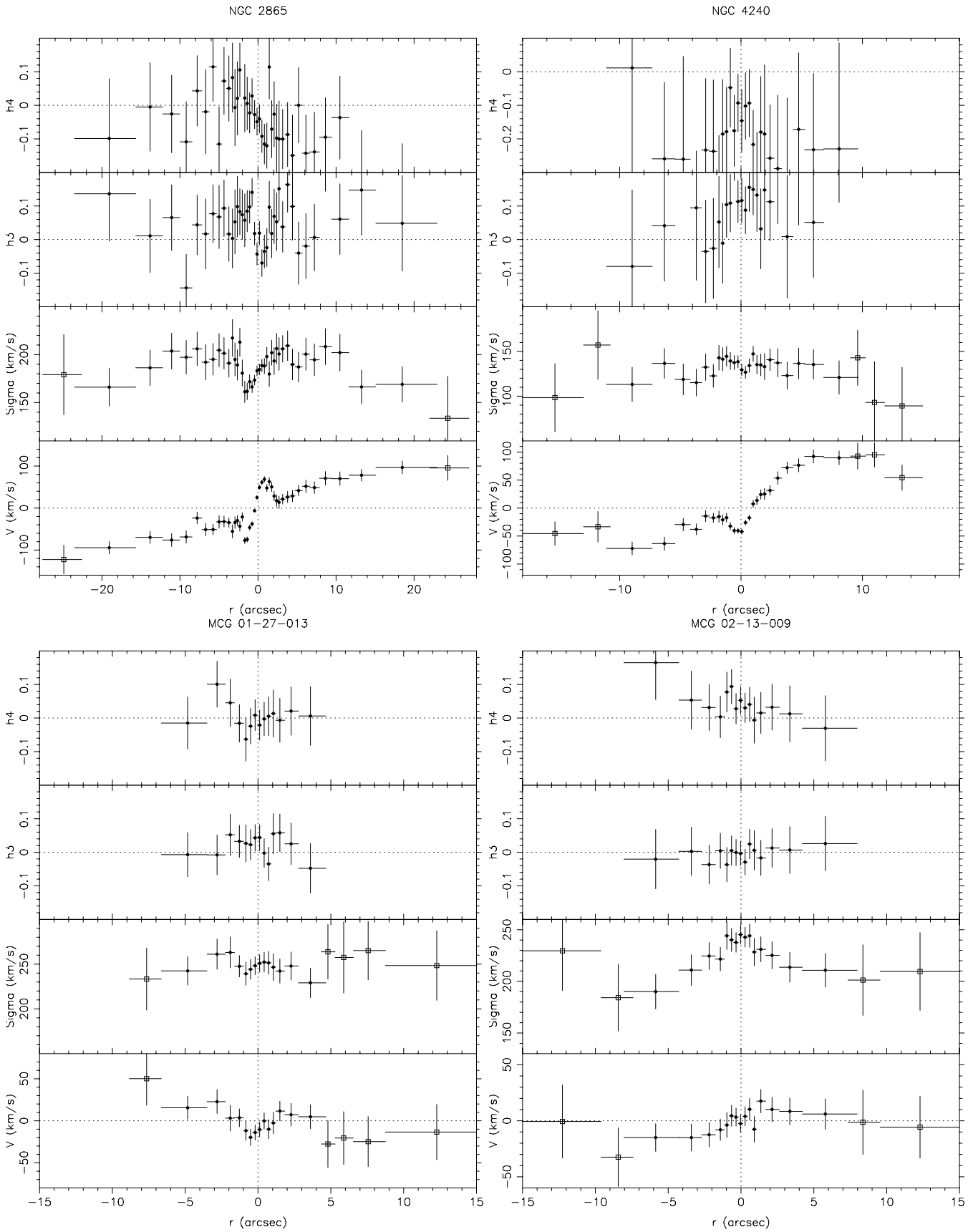

Figure 3. Radial kinematic profiles of isolated galaxies. From bottom to top are shown rotation velocity, velocity dispersion, third and fourth hermite terms. The open symbols indicate lower-S/N data for which we do not calculate hermite terms.

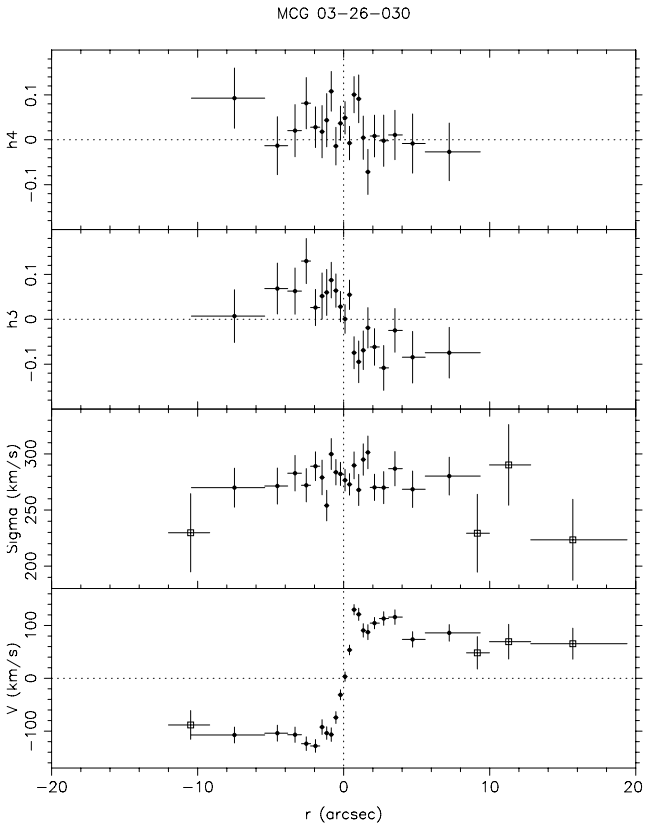

Figure 4. Radial kinematic profiles of MCG-03-26-030. From bottom to top are shown rotation velocity, velocity dispersion, third and fourth hermite terms. The open symbols indicate lower-S/N data for which we do not calculate hermite terms.

We placed the slit along the minor axis for this galaxy. In this case, the velocity profile is generally consistent with no rotation in the outer regions. The inner regions suggest some velocity substructure but this could be due to a small misalignment of the slit by 1 arcsec or the major axis dust lane. The velocity dispersion profile is fairly flat within the inner region indicative of a rotating disc. The h_3 and h_4 terms are inconclusive.

4.2 ESO 218−G002

From the imaging study of Reda et al. (2004), ESO 218−G002 has a large PA twist in its isophotes but otherwise shows no obvious fine structure. ESO 218−G002 lies in the direction of the 'Great Attractor' (Dressler, Faber & Burstein 1991), and near the border of the so-called Norma cluster.

Along the slit at radii ≈15 arcsec on both sides of nucleus there is an excess of light due to faint sources which are too faint for redshift measurements. There is a faint, marginally resolved source with an emission-line spectrum at 21.2 arcsec from the galaxy nucleus. Its position measured from a b_J image of the SuperCosmos Sky Survey is $\alpha = 12^{\rm h}\,21^{\rm m}\,08\overset{\rm s}{.}26$, $\delta = -52^\circ\,35'\,30\overset{''}{.}8$ (J2000). Emission lines of Hγ, Hδ, Hβ and [O III] are present and the redshift measured from these is $z = 0.101$. Close to this source at $\alpha = 12^{\rm h}\,21^{\rm m}\,08\overset{\rm s}{.}44$, $\delta = -52^\circ\,35'\,35\overset{''}{.}3$ is another marginally resolved source which has no emission in its spectrum and we are unable to measure a redshift from its faint absorption-line spectrum. It may be possible that there is a background cluster in the vicinity of ESO 218−G002. At 83 arcsec from ESO 218−G002 there is an X-ray source (1RXS J122104.3−523617).

The velocity profile of ESO 218−G002 is roughly solid body but lop-sided. The rotation is slow, peaking at 44 km s^{-1}. The velocity dispersion rises towards the centre with a corresponding dip in the central h_3 profile.

4.3 ESO 318−G021

The galaxy shows no obvious fine structure (Reda et al. 2004). There is weak [O III] emission at the centre of the galaxy which is also slightly extended. The gas rotation is the same sense and same magnitude as the stars. There may also be some Hβ emission but it is weak and rotation is not obvious. There is strong Hβ absorption indicative of a young nuclear stellar population.

We find a smooth regular velocity profile, and declining velocity dispersion with radius. These properties are consistent with a fast rotator containing a disc. Within the errors both the h_3 and h_4 terms show relatively flat profiles.

4.4 NGC 682

The DSS and two-Micron All-Sky Survey (2MASS) imaging suggests a featureless elliptical. The velocity profile is lop-sided suggesting a possible central KDC of size 4 arcsec (1.4 kpc). In the same central regions, the velocity dispersion profile is relatively flat. The hermite terms suggest a non-equilibrium structure. We note that the spectrum was taken at an angle intermediate to the major and minor axes.

4.5 NGC 1045

NGC 1045 reveals a tidal plume, evidence for dust and boxy isophotes (Reda et al. 2004), suggestive of a recent merger. The velocity profile shows solid-body rotation rising to ∼100 km s^{-1} at our largest radii of ∼25 arcsec (7.3 kpc). The velocity dispersion is sharply peaked at the galaxy centre. The h_3 and h_4 profiles (and the inner rotation profile) suggest some velocity substructure.

4.6 NGC 1162

The DSS and 2MASS imaging suggest a featureless elliptical, with fairly round inner regions. The galaxy major axis is therefore difficult to define. We estimate a PA of around 51°, whereas we placed our slit on an intermediate axis of PA = 280°. The central regions show evidence for a rotating disc. The velocity dispersion profile reveals a dip in the central 3 arcsec.

4.7 NGC 2110

The galaxy is a well-known active galactic nucleus (e.g. Pfefferkorn, Boller & Rafanelli 2001) and appears in the isolated galaxy sample of Colbert, Mulchaey & Zabludoff (2001). Strong emission lines are seen, with a large spatial extension beyond the continuum. This may affect the kinematic values derived in the outer, lower-S/N region. Strong rotation is seen with a (off-centre) peaked velocity dispersion profile. Both hermite profiles appear to be fairly regular.

4.8 NGC 2271

The DSS and 2MASS imaging indicates an elongated ($\epsilon = 0.3$) early-type galaxy. Koprolin & Zeilinger (2000) have suggested that

Table 4. Kinematic measurements. The systemic velocity $V_{\rm system}$ is taken as the mean of the velocities measured for the spectra with S/N $\geqslant$ 30. The maximum rotational velocity $V_{\rm max}$ is taken as the difference of the most extreme velocity measurements for all data points. The central velocity dispersion σ_0 is taken as the measurement for the spatial bin closest to the galaxy centre. The anisotropy parameter $(V/\sigma_0)^*$ is defined as $(V_{\rm max}/\sigma_0)/\sqrt{\epsilon/1-\epsilon}$. Literature velocity dispersions come from Hyperleda.

Galaxy	$V_{\rm system}$ (km s^{-1})	$V_{\rm max}$ (km s^{-1})	σ_0 (km s^{-1})	$(V/\sigma_0)^*$	σ_0 (literature) (km s^{-1})
ESO 153−G003	6341.5	42.7 ± 18.8	222.5 ± 11.9	0.19 ± 0.09	–
ESO 218−G002	4251.3	44.0 ± 7.4	297.9 ± 11.2	0.30 ± 0.06	235
ESO 318−G021	4793.3	152.9 ± 16.5	256.5 ± 8.9	0.92 ± 0.13	156
NGC 682	5436.8	74.5 ± 12.6	199.4 ± 4.7	0.58 ± 0.11	–
NGC 1045	4462.4	106.4 ± 17.6	286.1 ± 5.1	0.57 ± 0.10	–
NGC 1162	3752.3	103.9 ± 4.7	208.3 ± 5.3	1.52 ± 0.11	–
NGC 2110	2326.3	168.5 ± 10.3	230.8 ± 11.4	1.46 ± 0.16	246
NGC 2271	2560.6	245.2 ± 11.5	260.3 ± 10.3	1.45 ± 0.12	148
NGC 2865	2558.1	109.7 ± 7.7	183.1 ± 5.3	1.20 ± 0.12	170
NGC 4240	1878.6	83.6 ± 12.3	129.4 ± 6.4	1.96 ± 0.38	–
MCG-01-27-013	9051.5	38.9 ± 14.0	250.9 ± 9.8	0.17 ± 0.07	–
MCG-02-13-009	5533.9	25.0 ± 14.1	245.2 ± 9.2	0.31 ± 0.19	–
MCG-03-26-030	8925.0	129.0 ± 7.8	276.6 ± 9.6	0.80 ± 0.08	–

NGC 2271 contains a KDC within the central 1.5 arcsec although it is not obvious from their kinematic profiles. They measure a rotation between the flat part of the rotation curve and the central regions of 263 ± 36 km s^{-1} and a velocity dispersion within the central 5 arcsec of $\sigma_0 = 237 \pm 7$ km s^{-1}. The $(V/\sigma)^* = 1.72 \pm 0.24$, which suggests an anisotropic rotator. We measure a maximum velocity of 245 ± 12 km s^{-1} and $\sigma_0 = 260 \pm 10$ km s^{-1}. The resulting $(V/\sigma)^* = 1.44 \pm 0.12$ (see Table 4).

We find a smooth regular velocity profile, and declining velocity dispersion. The rotation reaches a high value of 245 km s^{-1}. The h_3 profile generally supports the presence of a disc. We are unable to confirm the claim of Koprolin & Zeilinger (2000) of a KDC in NGC 2271.

4.9 NGC 2865

This galaxy contains dust and shells (Reda et al. 2004) and is an excellent candidate for a merger remnant (Hau, Carter & Balcells 1999). Koprolin & Zeilinger (2000) measure little or no rotation of 72 ± 15 km s^{-1}, $\sigma_0 = 184 \pm 5$ km s^{-1}, and $V/\sigma)^* = 0.67 \pm 0.14$. We measure a maximum velocity of 110 ± 8 km s^{-1} and $\sigma_0 = 183 \pm 5$ km s^{-1}. Combined with an assumed ellipticity of 0.2 gives $(V/\sigma)^* = 1.20 \pm 0.12$ (see Table 4).

The velocity profile shows a clear signature of a KDC in the central 4 arcsec (6.4 kpc) and solid-body rotation in the outer regions. Within the same central region, the velocity dispersion reveals a strong dip from ∼200 to 160 km s^{-1}. The h_3 and h_4 profiles are quite distorted indicating a non-equilibrium situation.

4.10 NGC 4240

The DSS imaging suggests a featureless, nearly round elliptical with a nearby bright star to the West. The galaxy reveals a KDC in the central 4 arcsec (5.0 kpc) and a lop-sided rotation (i.e. 100 versus 50 km s^{-1}). The velocity dispersion profile is quite flat. The h_3 and h_4 profiles peak at the galaxy centre.

4.11 MCG-01-27-013

The DSS and 2MASS imaging suggest a featureless elliptical. The velocity profile reveals evidence for a weak KDC within 5 arcsec (2.9 kpc) and little or no rotation in the outer regions. The velocity dispersion profile is fairly constant with radius. The hermite profiles indicate a non-equilibrium structure.

4.12 MCG-02-13-009

The DSS imaging indicates several faint galaxies, but redshifts are not available for them. The galaxy has E+A type spectra and [O III] emission. The galaxy shows some evidence of slow rotation in the inner regions but is consistent with no rotation in the outer parts. A centrally peaked velocity dispersion profile is seen.

4.13 MCG-03-26-030

The imaging study of Reda et al. (2004) found this galaxy to have discy isophotes. The velocity profile shows evidence for rapid rotation in the inner 4 arcsec (2.3 kpc), reaching a constant velocity of almost 100 km s^{-1} in the outer regions. The velocity dispersion is fairly constant. The h_3 term shows a symmetric profile indicating a discy component is present.

5 DISCUSSION

The internal kinematics of early-type galaxies has been investigated by several authors in the past (e.g. Franx, Illingworth & Heckman 1989; Bender, Saglia & Gerhard 1994; Mehlert et al. 1998; Koprolin & Zeilinger 2000). Recently, this has included 2D kinematics via integral field units (e.g. Cappellari et al. 2005). Most of these previous studies covered early-type galaxies in clusters and groups – none focused on isolated galaxies. KDCs are thought to be small, rapidly rotating discs at the centres of these galaxies, although they are very difficult to detect photometrically (Forbes, Franx & Illingworth 1995).

Excluding our one minor-axis observation, the remaining dozen galaxies reveal evidence for a KDC or velocity substructure in five cases (an additional KDC has been claimed in NGC 2271 but it is not seen in our data). Thus, KDCs are fairly common in isolated galaxies at around 40 per cent.

From these studies of galaxies in high-density environments, the incidence of KDCs is observed to be about 33 per cent (rising to 50 per cent when projection effects are considered). Thus we find a

similar, possibly even higher, fraction in isolated galaxies. Koprolin & Zeilinger (2000) found typical KDC radii of 0.4 kpc. For our sample, which is on average two to three times more distant than the Koprolin & Keilinger sample, we find the KDCs to have diameter sizes of a few kpc. KDCs in galaxies located in high-density environments are generally found to be old and hence long-lived systems (Kuntschner et al. in preparation). We note that the KDC in NGC 2865 with an age of $\leqslant$1 Gyr (Hau et al. 1999) is an exception. A future paper will explore radial stellar population trends, and derive KDC ages, for this sample of 13 galaxies. KDCs are generally thought to be the result of a major merger (Hernquist & Barnes 1991), however they may also form in an early collapse without subsequent mergers (Harsoula & Voglis 1998).

The anisotropy parameter $(V/\sigma)^*$ can be used to separate galaxies that are rotationally supported (generally low luminosity) from those that are anisotropic (generally high luminosity). The division occurs around $(V/\sigma)^* = 0.7$ (Bender, Burstein & Faber 1992). Our sample of 13 galaxies follow the trends seen for larger samples (e.g. Davies et al. 1983; Bender et al. 1992; Koprolin & Zeilinger 2000). Although as Fig. 5 shows, our sample reveals a wide range of anisotropy values for a small range in galaxy magnitude. This general trend has been interpreted as a change in the merger progenitor type from gaseous (wet) mergers of spirals to the gas-free (dry) mergers of ellipticals (Naab, Khochfar & Burkert 2005). Perhaps the only notable exception is MCG-03-26-030 which appears to be a high-luminosity galaxy ($M_B = -21.5$) that is rotationally supported. There is evidence for a disc in the kinematic profile of this galaxy (see Fig. 4).

As noted in Section 1, Weil & Hernquist (1996) have predicted that remnants of multiple major mergers (e.g. a merged small group) will reveal rotation about the minor axis and an increasing V/σ with galactocentric radius. In virtually all cases (the exception being ESO 153−G003 where we placed the slit along the minor axis) our isolated galaxy sample reveals both of these properties. However, we note that such properties are also commonly seen in ellipticals in higher-density environments (e.g. Koprolin & Zeilinger 2000). The strongest kinematic differences between pair and multiple mergers are predicted to arise at three to four effective radii, i.e. well beyond the radii that current long-slit observations can explore. Perhaps the best argument against our sample being the remnants of merged groups is their modest optical luminosity. Only MCG-03-26-030 with $M_B = -21.5$ is bright enough to be a possible small 'fossil' group (see Jones et al. 2000).

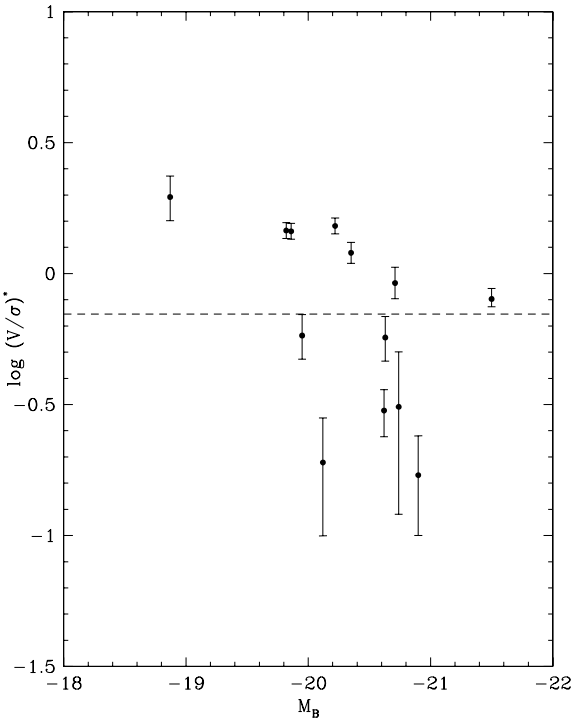

Figure 5. Anisotropy–luminosity diagram. Anisotropy parameter as a function of galaxy *B*-band luminosity for isolated galaxies. The horizontal dashed line shows the separation between rotation supported galaxies and anisotropic ones as given by Bender et al. (1992). Our small sample is consistent with the general trends for galaxies in higher-density environments.

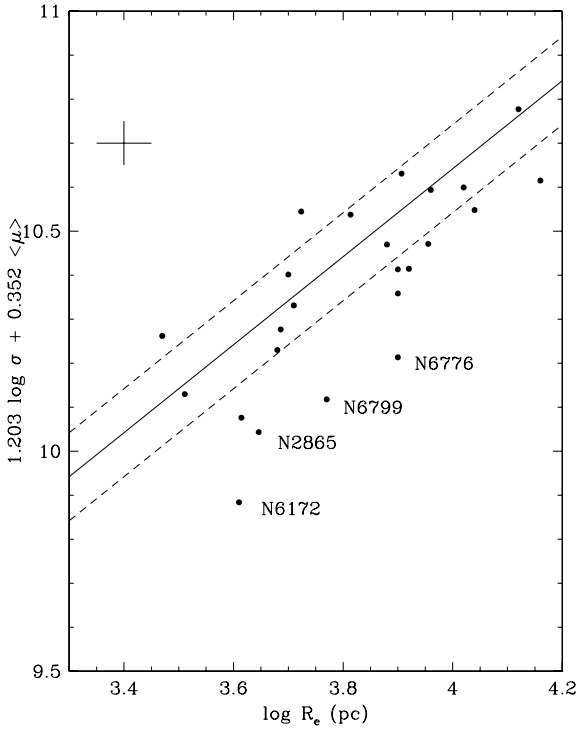

Figure 6. FP for isolated galaxies. Isolated galaxies shown are from this work and from Reda et al. (2005). The solid and dashed lines show the Coma cluster relation and dispersion from Jørgensen et al. (1993). Isolated galaxies reveal a similar FP to those of cluster ellipticals, albeit with somewhat larger scatter. Four particularly deviant galaxies are labelled (see text for details).

In Fig. 6, we show the FP for isolated galaxies compared to Coma cluster ellipticals (Jørgensen, Franx & Kjærgaard 1993). For the isolated galaxies, we include the galaxies studied in this work plus those from Reda et al. (2005) where available. The plot shows that isolated galaxies generally follow the FP of ellipticals in the higher-density environment of the Coma cluster with a slightly larger scatter ($\sim$0.15 dex compared to 0.1 dex) and offset by -0.1 dex. Four galaxies in particular are strongly offset from the mean FP (i.e. NGC 2865, 6172, 6776 and 6799). This offset can be understood in terms of their young stellar populations and hence reduced mass-to-light ratio (Forbes et al. 1998). The offset in the remaining galaxies could be a stellar population effect or a small calibration offset.

6 CONCLUSIONS

We have derived rotation velocity, velocity dispersion and hermite radial profiles for 13 isolated early-type galaxies. These profiles extend to $\sim$1 effective radius, or half of the enclosed galaxy mass. We

observe a dichotomy in kinematic properties similar to that in the elliptical population as a whole, where rotational support tends to be found in low-luminosity ellipticals. For all galaxies the V/σ ratio increases with radius. We find KDCs or velocity substructure in $\sim$40 per cent of the galaxies for which we have major axis spectra. Such a fraction is similar to that observed for ellipticals in higher-density environments. Most galaxies in the sample reveal kinematic evidence for a nuclear disc. The non-relaxed kinematics in several galaxies suggests that they have undergone mergers or accretion events. Isolated ellipticals generally follow the FP defined by cluster ellipticals – exceptions being those galaxies with evidence for young stellar populations. Overall, isolated ellipticals have similar kinematic properties to their counterparts in higher-density environments. Our conclusions support those from our previous papers on isolated galaxies, i.e. Reda et al. (2004, 2005).

ACKNOWLEDGMENTS

We thank R. van der Marel for his spectral analysis code. We also thank R. Proctor and S. Brough for their help carrying out some of the observations. We thank F. Reda and S. Brough for useful comments on the text. DAF thanks the ARC for partial financial support.

REFERENCES

Bender R., Burstein D., Faber S. M., 1992, ApJ, 399, 462
Bender R., Saglia R., Gerhard O., 1994, MNRAS, 269, 785
Cappellari M. et al., 2005, preprint (astro-ph/0509470)
Colbert J. W., Mulchaey J. S., Zabludoff A. I., 2001, AJ, 121, 808
Davies R., Efstathiou G., Fall S., Illingworth G., Schechter P., 1983, ApJ, 266, 41
de Lucia G., Springel V., White S. D. M., Croton D., Kauffmann G., 2006, MNRAS, 366, 499
D'Onghia E., Sommer-Larsen J., Romeo A. D., Burkert A., Pedersen K., Portinari L., Rasmussen J., 2005, ApJ, 630, L109
Dressler A., Faber S., Burstein D., 1991, ApJ, 368, 54
Forbes D. A., Franx M., Illingworth G., 1995, AJ, 109, 1988
Forbes D. A., Ponman T. J., Brown R. J. N., 1998, ApJ, 508, L43
Forbes D. A., Terlevich A. I., 2001, in ASP Conf. Ser., Vol. 209, Small Galaxy Groups: IAU Colloquium 174. Astron. Soc. Pac., San Francisco, p. 335
Franx M., Illingworth G., Heckman T., 1989, AJ, 98, 538
Garcia A. M., 1993, A&AS, 100, 47
Harsoula M., Voglis N., 1998, A&A, 335, 431
Hau G. K. T., Carter D., Balcells M., 1999, MNRAS, 306, 487
Hernquist L., Barnes J., 1991, Nat, 354, 210
Jones L. R., Ponman T. J., Forbes D. A., 2000, MNRAS, 312, 139
Jørgensen I., Franx M., Kjærgaard P., 1993, ApJ, 411, 34
Jørgensen I., Franx M., Kjærgaard P., 1995, MNRAS, 276, 1341
Kauffmann G., Charlot S., 1998, MNRAS, 287, L23
Koprolin W., Zeilinger W., 2000, A&A, 145, 71
Kuntschner H., Smith R. J., Colless M., Davies R. L., Kaldare R., Vazdekis A., 2002, MNRAS, 337, 172
Marcum P. M., Aars C. E., Fanelli M. N., 2004, AJ, 127, 3213
Mehlert D., Saglia R., Bender R., Wegner G., 1998, A&A, 332, 33
Naab T., Khochfar S., Burkert A., 2005, ApJ, 636, L81
Nagashima M., Lacey C. G., Okamoto T., Baugh C. M., Frenk C. S., Cole S., 2005, preprint (astro-ph/0504618)
Pfefferkorn F., Boller Th., Rafanelli P., 2001, A&A, 368, 797
Reda F. M., Forbes D. A., Beasley M., O'Sullivan E. J., Goudfrooij P., 2004, MNRAS, 354, 851
Reda F. M., Forbes D. A., Hau G. K. T. 2005, MNRAS, 360, 693
van der Marel R., 1994, MNRAS, 270, 271
van der Marel R., Franx M., 1993, ApJ, 407, 525
Weil M., Hernquist L., 1996, ApJ, 460, 101.

This paper has been typeset from a TEX/LATEX file prepared by the author.